

Seismically observed seiching in the Panama Canal

D. E. McNamara,¹ A. T. Ringler,¹ C. R. Hutt,¹ and L. S. Gee¹

Received 12 August 2010; revised 7 January 2011; accepted 1 February 2011; published 21 April 2011.

[1] A large portion of the seismic noise spectrum is dominated by water wave energy coupled into the solid Earth. Distinct mechanisms of water wave induced ground motions are distinguished by their spectral content. For example, cultural noise is generally <1 s period, microseisms dominate the seismic spectrum from periods of 2 to 20 s, and the Earth's "hum" is in the range of 50 to 600 s. We show that in a large lake in the Panama Canal there is an additional source of long-period noise generated by standing water waves, seiches, induced by disturbances such as passing ships and wind pressure. We compare seismic waveforms to water level records and relate these observations to changes in local tilt and gravity due to an oscillating seiche. The methods and observations discussed in this paper provide a first step toward quantifying the impact of water inundation as recorded by seismometers. This type of quantified understanding of water inundation will help in future estimates of similar phenomena such as the seismic observations of tsunami impact.

Citation: McNamara, D. E., A. T. Ringler, C. R. Hutt, and L. S. Gee (2011), Seismically observed seiching in the Panama Canal, *J. Geophys. Res.*, 116, B04312, doi:10.1029/2010JB007930.

1. Introduction

[2] The broadband power spectral density (PSD) of ambient noise at a seismic station is determined by a several different sources. At short periods (0.01–1 s) ambient noise levels are generally dominated by human-generated ("cultural") seismic energy radiated from the electrical grid, cars, trains, and machinery within a few kilometers of the recording station [McNamara and Buland, 2004]. Intermediate periods (2–20 s) are dominated by microseisms, which can be many orders of magnitude higher in power than other parts of the seismic spectrum. The largest microseism peak (5–10 s period) is the double-frequency microseism (DFM) that results from the nonlinear interaction of interfering ocean wave components producing a pressure pulse at double the water wave frequency [e.g., Bromirski, 2009]. This pressure pulse propagates to the seafloor where it couples into the solid Earth as seismic waves. The DFM is thought to be generated both near coasts, where coastal swell reflection can provide the requisite opposing wave components, and in the deep ocean [Languet-Higgins, 1950; Bromirski and Duennebie, 2002]. A second, lower-power spectral peak (11–20 s), commonly called the primary or single-frequency microseism (SFM), arises from the transfer of ocean gravity wave (swell) energy to seismic waves as ocean waves shoal and break in shallow coastal waters. The highest-amplitude and longest-period breaking swells are created by large and intense storms that generate strong sustained winds over a large area [Hasselmann, 1963; Aster et al., 2008]. Long-period (50–600 s) signals are generally caused by ocean infragravity waves generated by storm-forced shoreward

propagating swells interacting with continental coastlines. These oceanic waves are commonly referred to as the "hum" of the Earth [Rhie and Romanowicz, 2004]. Hum amplitudes are connected to ocean swell wave heights and are often related to climate [Bromirski, 2009].

[3] The broadband ambient seismic noise spectrum is thus multimodal with distinctly different physical mechanisms transferring cultural and water wave energy to seismic waves in the solid Earth. In this study, we demonstrate an example of station specific long-period noise (100–200 s) caused by flexure of the solid Earth in response to a standing water wave, also called a seiche, in a portion of a large lake in the Panama Canal. Good correlation between long-period seismic noise with local wind speed observations and shipping traffic in the Panama canal allow us to suggest possible seiche forcing mechanisms.

2. Site and Data Description

[4] We analyze 3.5 years of continuous broadband digital seismic time series from station CU.BCIP (Figure 1a). CU.BCIP is operated by the U.S. Geological Survey (USGS) as part of the Global Seismographic Network (GSN) and is located at the Smithsonian Tropical Research Institute (STRI) on Barro Colorado Island (BCI) in Lake Gatun in the Panama Canal (Figure 1b). The Panama Canal system is an 80 km long waterway that joins the Caribbean Sea in the north to the Pacific Ocean in the south (Figure 1b). It is composed of locks and excavated canal segments connecting a large central lake to the sea on either coast. BCI was a hilltop that became an island as a result of the flooding of 425 km² Lake Gatun during the construction of the Panama Canal system in 1907 [Pabst, 2000]. BCI spans much of Lake Gatun at its location so that the island is effectively bounded by relatively narrow channels on all sides, with the deeper channel on BCI's north and east sides, where the main shipping route lies ("main shipping channel" in Figure 1c).

¹Albuquerque Seismological Laboratory, USGS, Golden, Colorado, USA.

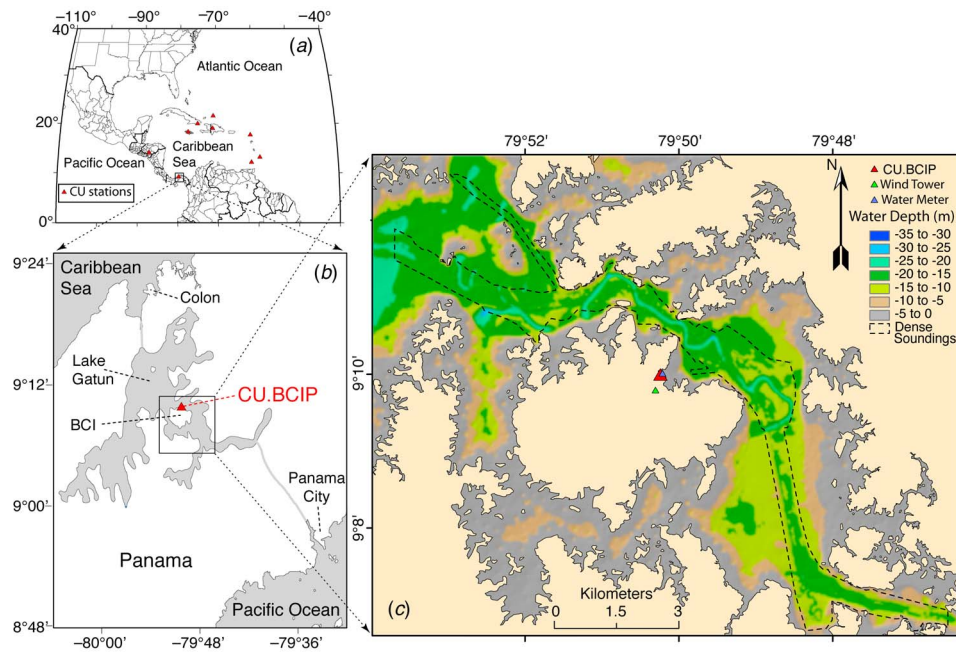


Figure 1. (a) Regional map of the Caribbean region. Red triangles are stations in the U.S. Geological Survey (USGS) Caribbean network (CU) including CU.BCIP [McNamara *et al.*, 2006]. (b) Map of the Panama Canal system including Lake Gatun, Barro Colorado Island (BCI), the Caribbean Sea, and the Pacific Ocean. (c) Bathymetry of the Panama Canal main shipping channel adjacent to BCI.

[5] Station CU.BCIP was installed in November 2006 as a part of a nine-station Caribbean network (network code: CU) in response to the M_W 9.15 Sumatra-Andaman Islands earthquake of 26 December 2004, after which domestic awareness of the destructive hazard posed by earthquakes and tsunamis increased [McNamara *et al.*, 2006]. Instrumentation at CU.BCIP (channel naming conventions after Ahern *et al.* [2007]) consists of a Quanterra Q330HR digitizer, an STS-2 broadband seismometer, an Episensor accelerometer, and real-time satellite communications, consistent with the standards of the Advanced National Seismic System (ANSS) “backbone” network [McMillan, 2002]. Ground motion sensors and communication system electronics are housed three meters underground in a large waterproof vault in order to achieve good coupling in the saturated rainforest floor and to protect equipment from damage due to excessive moisture (station information can be found at; <http://earthquake.usgs.gov/monitoring/operations/station.php?network=CU&station=BCIP>).

[6] Continuous seismic data and corresponding metadata for CU.BCIP were retrieved from the online archives of the USGS Albuquerque Seismological Laboratory (ASL) Data Collection Center (DCC). Duplicate data are archived and distributed by the Incorporated Research Institutions for Seismology (IRIS) Data Management Center (DMC; <http://www.iris.edu/data/>).

3. Spectral Methods and Observations

3.1. Spectral Processing

[7] In our analysis, the variation of long-period spectral power is observed by computing instrument corrected power spectral density (PSD) probability density functions (PDFs) using the methods presented by McNamara and Buland

[2004]. PSD methods follow the original algorithm used to develop the GSN New Low- and High-Noise Models (NLNM, NHHM) [Peterson, 1993]. PSDs are computed from continuous, 50% overlapping time series segments (BH channels: 1 h segments sampled at 40 samples per second (sps); LH channels: 3 h segments sampled at 1 sps. All available data are included; there is no removal of high-power transients due to earthquakes and instrumentation problems. The instrument transfer function is deconvolved from each time segment, yielding ground acceleration. Each time series segment is divided into 13 subsegments (of 360 s for BH channels and 2700 s for LH channels); these subsegments overlap by 75%. Each subsegment is processed by (1) removing the mean, (2) removing the long-period trend, (3) cosine tapering 10% of each end of the subsegment, (4) transforming *via* Fast Fourier Transform (FFT) to obtain an amplitude spectrum, and (5) squaring the amplitude spectrum to obtain a PSD. The final PSD estimate is calculated as the ensemble average of the 13 subsegment PSDs. Subsegment averaging reduces variance such that the PSD has a 95% level of confidence that the spectral point lies within -2.14 dB to $+2.87$ dB of the estimate. The averaged PSD is then smoothed by computing full-octave averages centered every one-eighth octave resulting in 96 spectral estimates from the Nyquist period to the longest resolved period (172 s for BH channels and 940 s for LH channels). PSDs are then combined into PDFs such that the distribution of spectral power is readily visualized [McNamara and Buland, 2004] (Figure 2).

3.2. Spectral Distribution of Power at CU.BCIP

[8] In order to produce a very broadband view of ambient noise characteristics at CU.BCIP, the broadband and

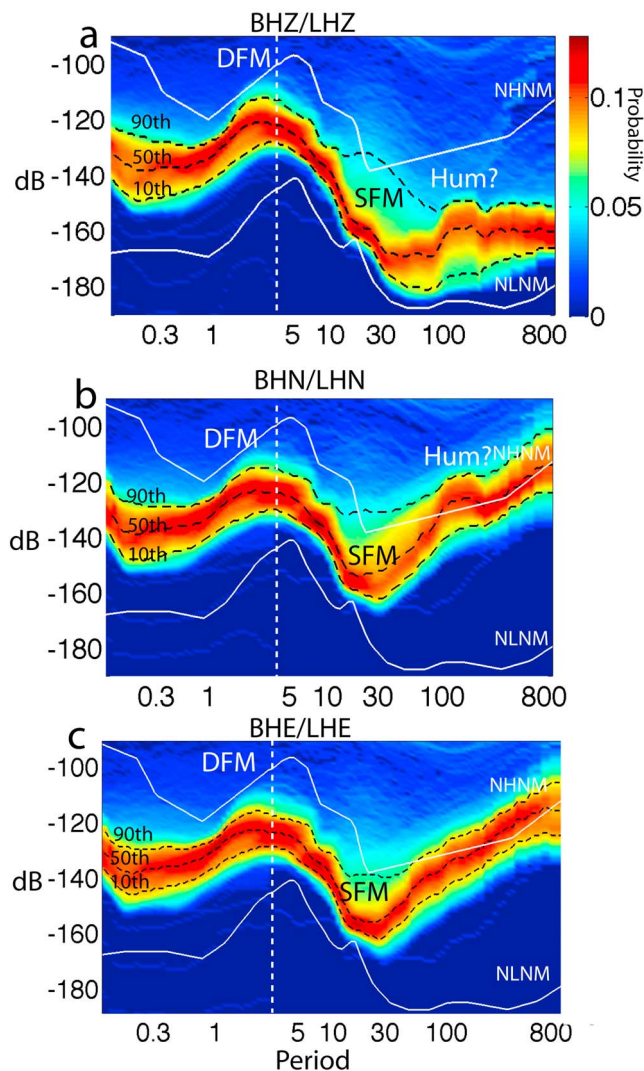


Figure 2. (a) Vertical component composite power spectral density (PSD) probability density functions (PDFs) showing the distribution of 54,364 one-hour PSDs for CU.BCIP.–.BHZ and 17,711 three-hour PSDs for CU.BCIP.–.LHZ, from 3 December 2006 to 10 February 2010. (b) Horizontal component composite PSD PDF showing the distribution of 54,500 one-hour PSDs for CU.BCIP.–.BHN and 17,673 three-hour PSDs for CU.BCIP.–.LHN over the same interval. (c) Composite PSD PDF showing the distribution of 54,500 one-hour PSDs for CU.BCIP.–.BHE and 17,673 three-hour PSDs for CU.BCIP.–.LHE. Major noise sources are labeled in their respective period bands: double-frequency microseism (DFM), single-frequency microseism (SFM), and Earth hum. The tenth, fiftieth, and ninetieth PDF probability percentiles are shown as dashed black lines [McNamara *et al.*, 2009]. The new low-noise (NLNM) and high-noise (NHNM) models of Peterson [1993] are shown for reference. The vertical white dashed line is the period where the BH and LH components are joined to make the composite PSD PDF.

long-period component PSD PDFs are merged at 3 s period and combined into a single composite PSD PDF for each component of motion. Figure 2a is a long-term composite PSD PDF showing the distribution of 54,364 PSDs for CU.BCIP.–.BHZ and 17,711 PSDs for CU.BCIP.–.LHZ, from 03 December 2006 to 10 February 2010. The period where BHZ and LHZ components are joined to produce the composite PSD PDF is marked by a vertical white dashed line (Figure 2). The north-south horizontal components (BHN and LHN) composite PSD PDF is shown in Figure 2b and BHE/LHE composite PSD PDF is shown in Figure 2c. As expected and observed at all global seismic stations, microseisms are the dominant ambient noise signal. On the CU.BCIP vertical component composite PSD PDF we also observe a very distinct spectral peak, from 100–200 s period (Figure 2a). Despite the high long-period noise levels on the horizontal components (BHN and LHN) (Figure 2b), the 100–200 s peak is well observed. Long-period noise levels are significantly higher so an isolated 100–200 s peak is not well observed on the BHE/LHE composite PSD PDF (Figure 2c). The 100–200 s spectral peak power levels on the vertical component (LHZ) are roughly 30 dB lower than on the horizontal components (LHN) yet still well observed because of lower vertical component ambient noise levels at adjacent periods.

3.3. Hum of the Earth

[9] The long-period seismic spectral band is generally occupied by the Earth's hum [Bromirski, 2009]. The Earth's hum signal is generally very low power and not well observed unless the recording seismic station has very good long-period noise characteristics [McNamara *et al.*, 2009]. In Figure 3 we show a composite PSD PDF for the vertical components of motion (BHZ and LHZ) at the GSN station in Tucson, Arizona, (IU.TUC.00; latitude = 32.31°N, longitude = 110.78°W). Spectral processing methods are the same as described above. Instrumentation at IU.TUC is a

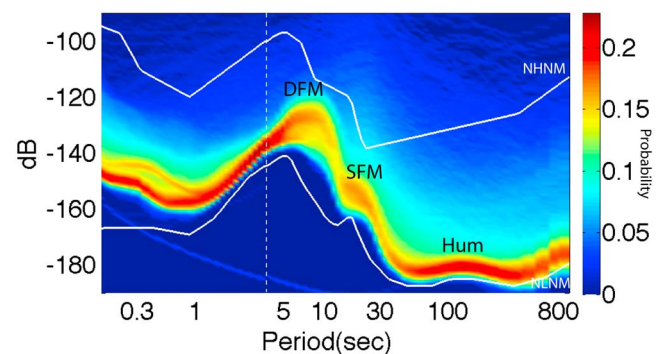


Figure 3. Vertical component composite PDF for a very quiet Global Seismographic Network station in Tucson, Arizona (IU.TUC), showing the distribution of 175,951 one-hour PSDs for the BHZ band and 98,684 three-hour PSDs for LHZ; the data span 6 November 1998 to 7 October 2009. Major noise sources and models are labeled as in Figure 2. The vertical white dashed line is the period where the BH and LH components are joined to make the composite PDF.

Streckeisen STS-1 in a buried vault that produces very good long-period noise characteristics. This is one of a small group of high-quality seismic stations with sufficiently low ambient noise levels to detect the hum [Bromirski, 2009]. The hum signal is very low power (near the NLNM) and has a broad smooth “bump” from ~50–600 s period. In contrast, signal in the same band, at CU.BCIP (Figure 2) has much higher power than IU.TUC suggesting that we observe anomalously high hum power levels at CU.BCIP or that the very high power long-period energy is from a different source altogether.

3.4. Temporal Distribution of Spectral Power at BCIP

[10] The long-period portion of the seismic spectrum containing the hum is generally observed to display seasonal variations that are consistent with the microseisms. Specifically, spectral power increases during the winter storm season when ocean wave activity produces higher seismic energy as they crash along coastlines [Ekström, 2001; Bromirski, 2009; Aster et al., 2008; Aster et al., 2010] and/or from standing waves in the deep ocean [Kedar et al., 2008]. In contrast, long-period seismic energy, recorded at CU.BCIP, does not display a strong seasonal power variation but instead has a strong diurnal signal. Following McNamara and Buland [2004], we gather spectral bins for each hour of the day using 17,711 three-hour PSDs for CU.BCIP.–LHZ from 03 December 2006 to 10 February 2010. The hourly bin PSD PDF median power as a function of period is plotted against time of day in Figure 4. For a broad range of periods, the highest powers occur during daytime hours (0600–1400 local time) and lowest powers in the early morning and nighttime hours (0000–0500 local time; Figure 4). Power averaged in the 100–200 s period band show diurnal variations on the order of 20 dB (Figure 4a). In Figure 4b we observe LHZ diurnal power variations, on the order of 10–20 dB, for a much broader range of periods that extend from 50–1000 s. In Figure 4c we show difference PSDs for all components between 1200 and 0200 local time. We observe a clear peak from 100–200 s on the LHZ component further indicating that in this period band, there is a roughly 20 dB increase in power level during the daytime. The LHN component displays a 10 dB increase during the daytime hours in the 100–200 s period band with a second peak centered near 40 s period. The LHE component shows the same general increase in power level during daytime hours however, over a broad range of periods that extend from 20–800 s.

[11] Diurnal spectral power variations observed in Figure 4 are corroborated with envelope functions computed using a single day of long-period band pass filtered (50–100 s period) seismic data recorded at CU.BCIP on 6 December 2009 (Figure 5a). On this typical day of data, strong diurnal power variation is readily observed with a minimum around 0000–0200 and maximum near 1000–1200 local time. In addition, we observe that the vertical component (LHZ) has significantly lower power than the horizontals (LHN and LHE; Figures 5a and 5b) and opposite polarity (Figure 5b). Long-period particle motion oscillates between down to the north-northeast and up to the south-southwest (Figure 5c).

[12] The observed diurnal variation of long-period spectral power, relative component amplitudes and particle motion are not typical of ambient noise due to oceanic microseisms and Hum [Bromirski, 2009]. For this reason we suspect that

the proximity of the Panama Canal to the CU.BCIP seismic station is of interest, and investigate local water action as the source of the long-period power characteristics. For the remainder of this study we will focus on modeling the amplitude of the most prominent 100–200 s spectral peak.

4. Modeling Water Waves as the Seismic Signal Source

4.1. Water Level Pressure Transducer Observations

[13] To investigate the source of the observed 100–200 s noise, we installed a temporary pressure transducer on the shore of BCI, approximately 30 m from the seismic station (Figure 1c). The water level meter (HOBO U2 Water Level Logger with a range of 0–4 m water depth) was installed on 29 February 2008 and ran for nearly 2 d. A full day of data for 1 March 2008 is shown with long-period seismic data for CU.BCIP.–LHZ (Figure 6). Both traces are band pass filtered from 100–200 s. As observed in the seismic data, the water level data show significant diurnal variation with greatest power during the daytime. We observe a very good correlation between water and seismic waves in 100–200 s period band (cross correlation coefficient = 0.95).

[14] The location of CU.BCIP within the Panama Canal system and the diurnal variation and coherence of seismic and water level amplitudes suggest that ship-generated wake waves interacting with the BCI shoreline might be responsible for the long-period (100–200 s) peak observed at CU.BCIP. However, in a study of waves generated by both conventional and high-speed passenger ferries at a beach close to the port of Mytilene (Island of Lesbos, Greece), *Velegrakis et al.* [2007] observed that ship wake wave spectra are dominated by energy in the band from 3 to 10 s period. Ambient seismic signals in this band generally are dominated by high-power double frequency (or secondary microseism) (DFM, Figures 2 and 3) that would likely obscure lower-power local wave sources. Freight ships, passing through the Panama Canal, are significantly larger than passenger ferries but are not expected to produce wake wave periods two orders of magnitude longer (100–200 s). For this reason we do not expect that ship wake waves will generate a long-period water wave that explains the 100–200 s period energy observed in the CU.BCIP seismic data (Figure 2).

4.2. Seiche

[15] The longest-period waves produced in enclosed bodies of water are standing waves, known as seiches [Simojoki, 1961]. Seiches generally are caused by resonances in a body of water disturbed by a variety of mechanisms that include: atmospheric pressure variations, wind [Keller and Stallard, 1994], ships [Joyce and Jewell, 2003], earthquakes [Ichinose et al., 2000], tsunamis [Foster and Karlstrom, 1967] and calving glaciers (J. M. Amundson et al., Dynamic iceberging processes and their role within the glacier-ocean system, submitted to Geophysical Research Letters, 2010). A standing wave can be represented by the sum of two waves travelling in opposite directions and reflecting from the ends of the basin. Superimposed traveling wave amplitudes result in vertical harmonic motion, an impulse that travels the length of the basin at a velocity that depends largely on the depth of the water. The direct relationship between the period of a

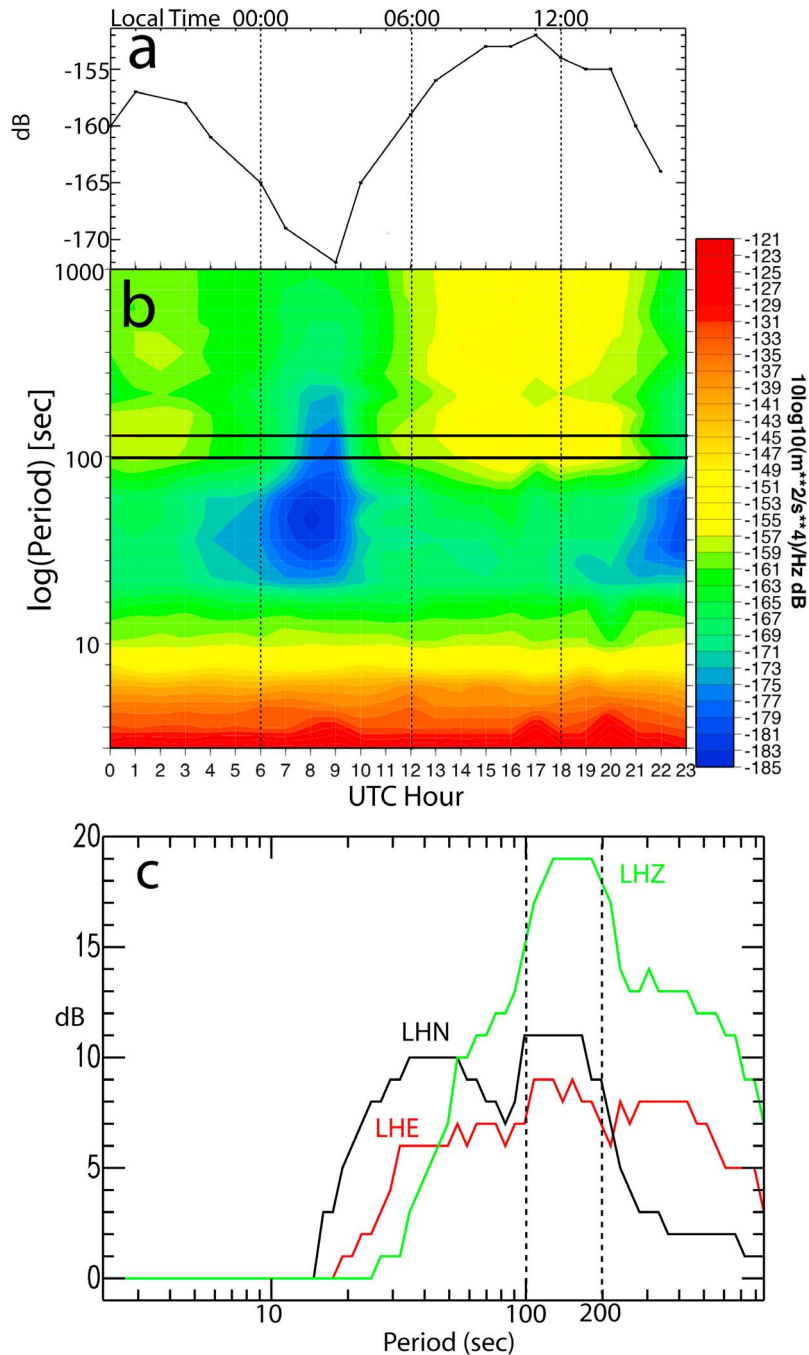


Figure 4. CU.BCIP.-LHZ diurnal variations. Hourly PDF bins are gathered from the PSD data shown in Figure 2. (a) Power variation averaged in the 100–200 s period band. (b) Hourly bin median power levels as a function of period and time are plotted. Strong diurnal signals are observed in a portion of the spectra with periods above 50 s; peak power is seen during the local daytime hours. Horizontal solid lines show the period band of 100–200 s signal. (c) Difference PSDs between 1200 and 0200 local time hourly PSD PDF medians.

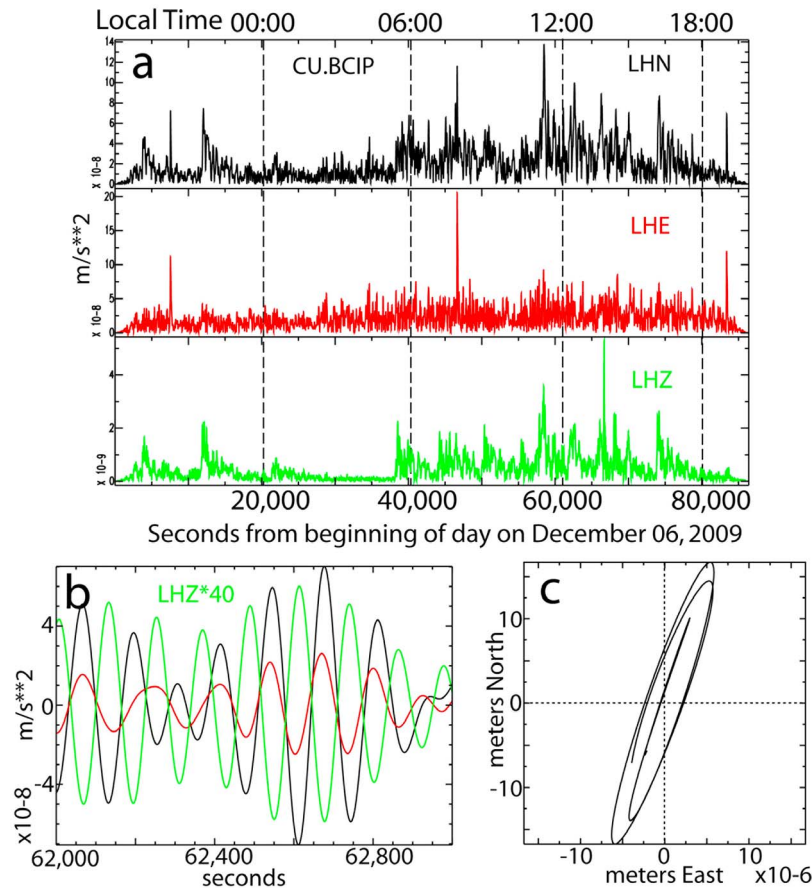


Figure 5. (a) Envelope functions computed for band pass filtered seismic data (filter corners at 50 and 1000 s period) recorded at CU.BCIP on 6 December 2009. The LHE component (red line) and LHN (black line) are significantly higher amplitude than the vertical component, LHZ (green line). (b) Detail of band pass filtered seismogram amplitudes (filter corners at 50 and 1000 s period) at 1200 local time. The LHZ component (green line) is multiplied by 40 in order to demonstrate polarity and amplitude differences between the three components of motion. (c) Horizontal particle motion displacement of a few cycles near the peak amplitude in Figure 5b.

seiche and the dimensions of the basin in which it takes place has been expressed by the formula of Merian [1828]

$$T = \frac{2L}{n\sqrt{\gamma h}} \quad (1)$$

where L is the length of the basin, h is the mean depth of the basin, γ is the acceleration of gravity ($\gamma \approx 9.81 \text{ m/s}^2$), and n is the number of nodal lines. Although equation (1) applies to a rectangular basin with uniform depth, it can be used as a first approximation for an irregular basin with a dominant dimension and known average depth [Rueda and Schladow, 2002].

[16] Since seiches are a common feature of semienclosed basins such as lakes, bays, gulfs, and harbors, we consider the case of a seiche in the main shipping channel of the Panama Canal northeast of BCI. Detailed channel depth data was obtained from the Panama Canal Commission Surveys of 1994 and is mapped in Figure 1c. For a reasonable range of channel dimensions adjacent to CU.BCIP (depths from 10 to

20 m and widths from 700 to 1500 m), the calculated dominant period of a fundamental mode seiche ($n = 1$) in this channel is between 89–302 s. This is slightly broader spectral range but consistent with the CU.BCIP observed seismic spectral power peak at 100–200 s (Figure 2).

[17] Another possibility is that the CU.BCIP 100–200 s period spectral peak (Figure 2) does not represent the fundamental mode of a seiche in the narrow shipping channel but is instead a higher-mode harmonic of some longer-period seiche that traverses the length of the full, surrounding portion of Lake Gatun. Lake Gatun long dimensions range from 5000–30,000 m (Figures 1a and 1b) and assuming similar water depths as the main shipping channel adjacent to BCI [Pabst, 2000], from equation (1) a Lake Gatun seiche could range from 500–1000 s period (Figure 7). This is consistent with diurnal power variations observed over a broad period range (Figures 4 and 5) and suggests that the 100–200 s PSD PDF peak could be due to higher-order harmonics of a longer-period Lake Gatun fundamental mode

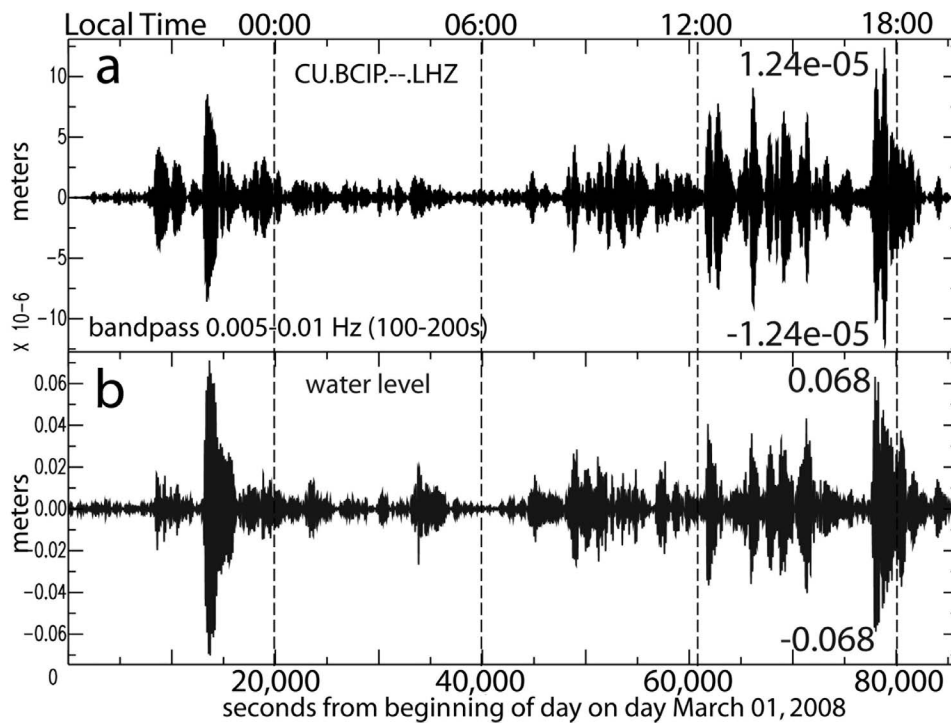


Figure 6. (a) Vertical displacement seismogram for 1 March 2008 from CU.BCIP--.LHZ. (b) Water height data recorded during the same interval. Both time series are band pass filtered (filter corners at 100 and 200 s period).

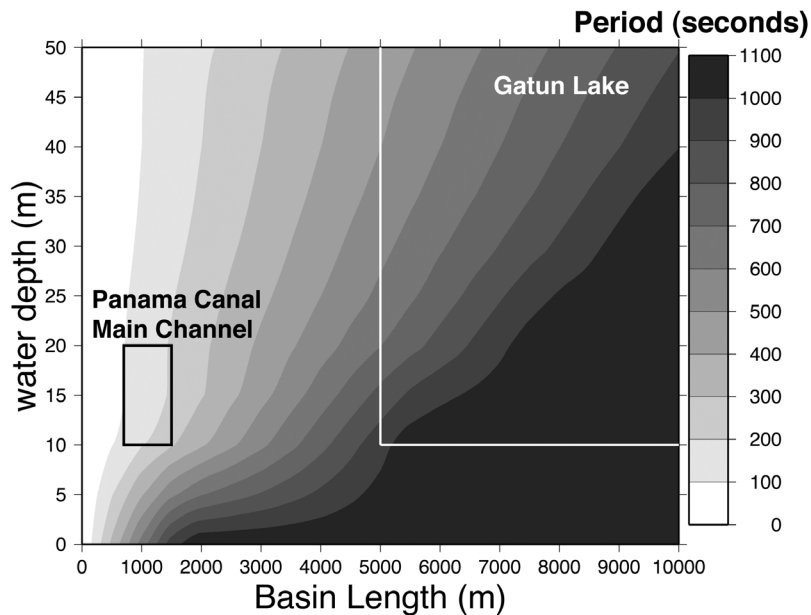


Figure 7. The relationship between seiche period and basin dimension, derived from the formula of Merian [1828]. For a reasonable range of Panama Canal main channel dimensions to the north and east of CU.BCIP (water depths from 10 to 20 m and widths from 700 to 1500 m), the calculated dominant period of a seiche, using equation (1), is between 89 and 302 s (black box). For a range of Lake Gatun dimensions (water depths >10 m and widths >5000) a Lake Gatun seiche period is roughly 600–1000 s (white box).

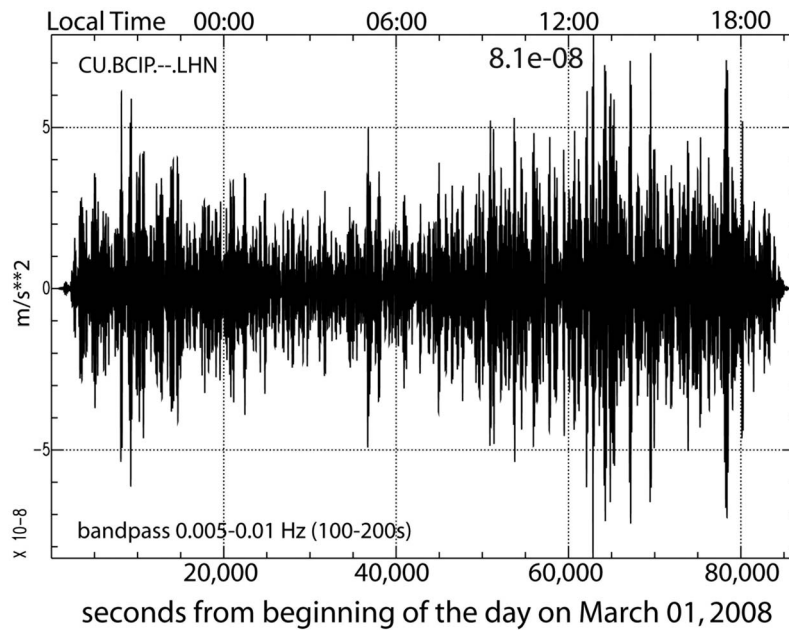


Figure 8. Horizontal component (LHN) band pass filtered accelerations for CU.BCIP.--LHN on 1 March 2008.

seiche. At this point it is difficult to distinguish between the two separate seiche sources however, CU.BCIP seismic observations suggest that the water level observed at BCI is driven by a seiche in either the adjacent main shipping channel northeast of BCI and/or the larger Lake Gatun, or both. To understand this explanation of the anomalous signal of CU.BCIP, we investigate several mechanisms by which a seiche in the Panama Canal could generate the observed seismic signal at CU.BCIP.

4.3. Modeling Vertical Acceleration Seismic Signal Due to Gravity

[18] Here we address whether a change in gravity due to the fluctuating water depth during a seiche can produce the horizontal, tilt-induced seismic signal observed at CU.BCIP. We estimate the associated Bouguer anomaly by assuming that BCI and the surrounding water can be approximated as concentric cylinders, with the radius of the island derived from a circle with area equivalent to the island's 15 km² surface area and a radius of the body of water similarly for a lake surface area of 425 km². The height of CU.BCIP is 4 m above the water surface and the density of water is 1000 kg/m³ [Turcotte and Schubert, 2002]. With these assumptions, the gravity change induced by a water depth fluctuation of ± 6.8 cm (Figure 6) is about 4.2×10^{-10} m/s². In contrast, the maximum observed horizontal acceleration on 1 March 2008 is 8.1×10^{-8} m/s² (Figure 8), nearly two orders of magnitude above the estimated Bouguer anomaly. From this result we conclude that signal caused by changes in gravity is a second-order effect and not the dominant long-period seismic signal source observed at CU.BCIP.

4.4. Modeling Vertical Displacement Seismic Signal Due to Flexure

[19] Next we will address how increased water height, due to a seiche, can couple energy into the solid Earth and produce

the long-period seismic vertical displacement signal observed at CU.BCIP. We model vertical displacement (and in section 4.5 also the apparent horizontal acceleration due to tilting the horizontal sensors within Earth's gravitational field) in response to water loading as an explanation for long-period seismic observations.

[20] Using well-established relationships, we estimate the physical parameters that describe the ground's response to the force of displaced water acting as a vertical point force (V_a). Specifically, we calculate the flexural tilt caused by a vertical point force acting on a one-dimensional beam [Turcotte and Schubert, 2002] (Figure 9). Vertical displacement (w) in this case is

$$w = \frac{V_a x^2}{2D} \left(L - \frac{x}{3} \right) \quad (2)$$

where $L = 2100$ m is the distance from the center of the idealized circular island and $x = L - 75 = 2025$ m is the distance to the seismometer from the center of BCI. The vertical force (V_a) in equation (2) is

$$V_a = \rho h r \quad (3)$$

where $r = L$ from equation (2), $\rho = 1000$ kg/m³ is the density of water, and $h_w = \pm 6.8$ cm is the height of water wave, taking the maximum water height on 1 March 2008 in Figure 6. We assume that loading is exclusively by this extra water and is applied at a single point near the water level pressure transducer just offshore of BCI (Figure 1c). Vertical displacement (w) is linearly dependent upon the vertical force (V_a) and is therefore not very sensitive to our estimate of the water loading. Flexural rigidity (D) in equation (2) is given by

$$D = \frac{Eh^3}{12(1 - \nu^2)} \quad (4)$$

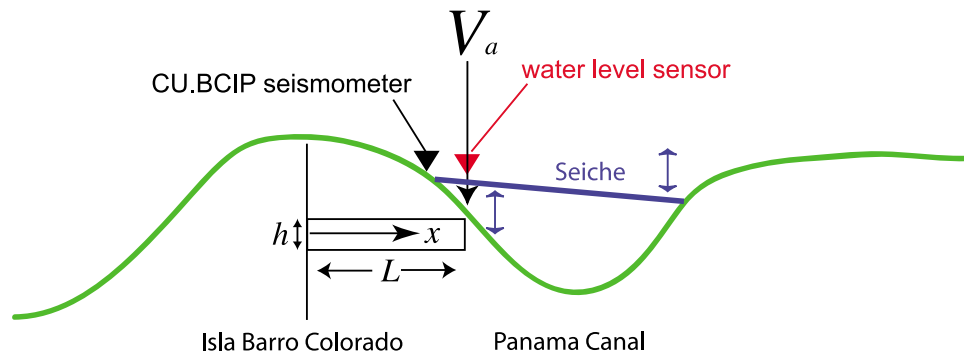


Figure 9. Cross section of Isla Barro Colorado and Panama Canal and schematic of beam flexure model with $L = 2100$ m (the distance from the water depth sensor) and $x = 2025$ m (the distance from the center of the island to the seismometer). The seiche water load is taken to act as a vertical point force, V_a , at the location of the water depth sensor.

We assume that the thickness of the flexing beam, $h = 10$ m, is comparable to the thickness of the easily deformed rainforest soil so that Young’s Modulus E represents a soft clay material, or about 0.25×10^9 Pa with a Poisson’s Ratio ν of about 0.5, a perfectly incompressible material bending elastically at small strains.

[21] Using the vertical point force V_a calculated from the maximum water height observed in Figure 6, we estimate a vertical soil surface displacement $w = 3.4 \times 10^{-5}$ m. At the time of maximum seismic amplitudes and water levels, about 1800, Figure 6 shows seismic displacement of about 1.2×10^{-5} m, so our flexure calculations overestimate the vertical displacement of the sensor by over a factor of two. We attribute part of this overestimate to using a vertical point load rather than a load distributed over a larger region, which would likely decrease our local displacement estimate but would remain of the same order of magnitude. Our overestimation does indicate that even our rather rough assumptions produce displacements of the same order of magnitude as the seismic observations. Given this very simple modeling approach, the factor of two is acceptable, and suggests that oscillating water in the Panama Canal can cause the observed vertical seismic displacements at CU.BCIP.

4.5. Modeling Horizontal Acceleration Seismic Signal Due to Tilt

[22] Seiche induced ground tilt has been observed by tilt meters and correlated to pressure-type tide gauge data in Aburatsubo Bay, Japan [Yanagisawa, 1980]. We infer that seiche-induced ground tilt may explain our long-period horizontal observations at CU.BCIP. (Note that these accelerations are not caused by translational motions of the seismometer but by tilting it within Earth’s gravitational field; such gravity/tilt signals on the horizontal components are $g \sin \theta$, where g is Earth’s surface gravitational acceleration, about 9.8 m/s^2 (J. Evans, personal communication, 2010). We now estimate the angles of rotation thus detected by the seismometer at CU.BCIP. Using observed displacement estimates from section 4.4 we can approximate the rotation angle simply by applying the linear vertical displacement Z , about 1×10^{-5} m, over a horizontal distance $X = 2025$ m from the center of BCI to the location of the water depth sensor at

its shoreline (Figure 10). Simple trigonometry yields an expected rotation angle θ as

$$\theta = \tan^{-1} \left(\frac{Z}{X} \right) \approx 2.8 \times 10^{-7} \text{ degrees} \quad (5)$$

The angle of tilt inferred from observed horizontal accelerations, if caused only by tilt with $\gamma = 9.81 \text{ m/s}^2$ for the peak acceleration at about 1800 in Figure 8 ($8.1 \times 10^{-8} \text{ m/s}^2$) is

$$\theta = \sin^{-1} \left(\frac{A}{g} \right) \approx 4.7 \times 10^{-7} \text{ degrees} \quad (6)$$

The angle of tilt computed is therefore within a factor of two of the estimated tilt angle from equation (6) for the peak horizontal acceleration in Figure 8. These results suggest that seiche-induced tilt of the solid Earth is a plausible explanation for seismic observations of 100–200 s

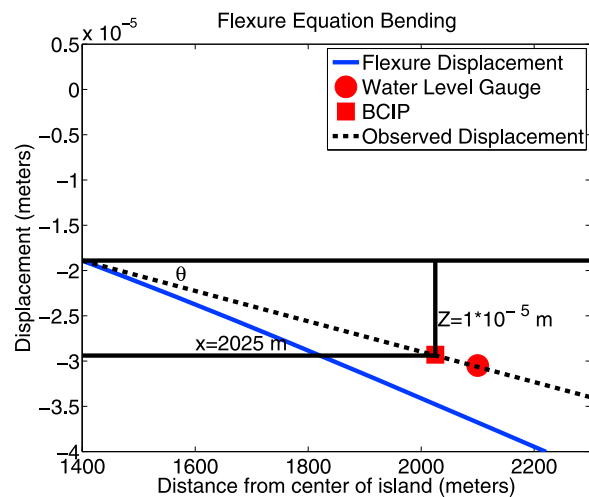


Figure 10. Displacement curve (blue line) based on vertical flexure calculations. Using vertical displacement estimates, we can approximate the tilt angle (θ) assuming a linear vertical displacement of $Z = 1 \times 10^{-5}$ m over a horizontal distance $X = 2025$ m.

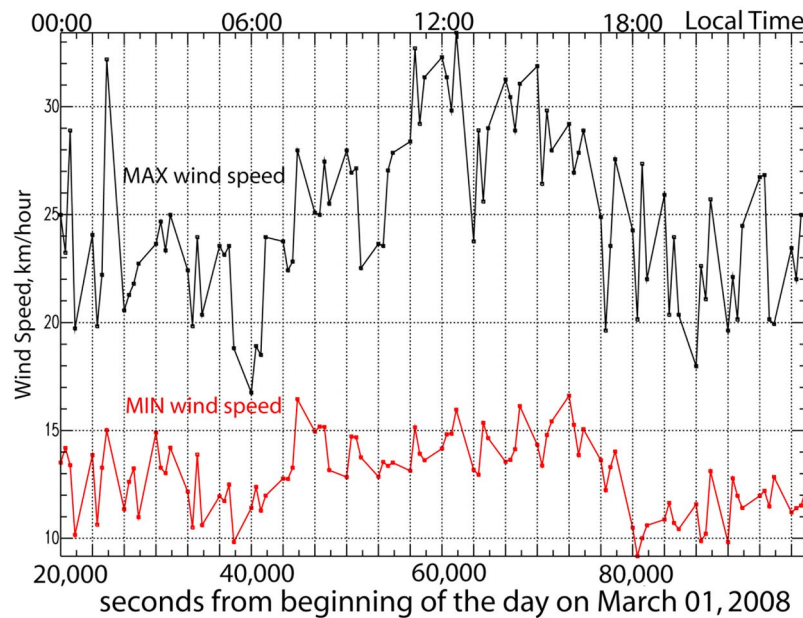


Figure 11. Wind speed (15 min interval minima (red line) and maxima (black line)) recorded at BCI over the same interval as Figures 5, 6, and 8 (1 March 2008).

vertical displacements and horizontal accelerations at CU.BCIP.

5. Discussion

5.1. Seiche Forcing Mechanisms

[23] Small rhythmic seiches are nearly ubiquitous in disturbed enclosed bodies of water and most often are caused by meteorological effects (wind and atmospheric pressure variations associated with winds), by seismic activity (earthquakes, tsunamis), or landslides. Seiches have been observed in large bodies of water because of seismic wave propagation from distant earthquakes. For example, shortly after the 22 January 2003 (0236:34) M7.6 earthquake in Colima, Mexico, a seiche was observed on Lake Pontchartrain Louisiana (http://neic.usgs.gov/neis/eq_depot/2003/eq_030122/). More often, seiches are generated by water surface disturbances through common forcing mechanisms. In section 4.5 we examined how a seiche couples energy into the solid Earth to produce observed long-period vertical displacement and apparent horizontal accelerations at CU.BCIP. We now discuss two possible forcing mechanisms for generating seiches and controlling temporal amplitude variations.

5.2. Ships

[24] Seismic noise associated with human activity, “cultural noise”, generally displays a strong diurnal variation with high power during the daylight working hours and relatively lower powers late at night when most people are sleeping and machinery is not operating. As discussed earlier, waves directly from ship wakes are very short period (3–10 s) and do not explain our long-period seismic observations [Velegrakis *et al.*, 2007]. However, it is reasonable to consider that the wakes of regular and frequent container ship traffic could cause the necessary disturbance to induce a standing wave

seiche in the main channel of the canal north of BCI. As passing ships disturb the water surface, standing waves could be induced by the summation of propagating wake waves, traveling in opposite directions, due to reflections off the opposite shorelines. As traveling wake waves constructively interfere, vertical harmonic motion results as gravity seeks to restore the horizontal surface of the water to a state of hydrostatic equilibrium.

[25] The Panama Canal operates continuously. However, traffic is heavier during daylight hours. In addition, the largest freight ships are only allowed to pass through the canal during daylight (<http://www.pancanal.com/eng/index.html>). The increased and often longer, heavier daytime ship traffic, in the Panama Canal, correlates well with the observed diurnal variation of spectral power and seiche height. Peak power occurs during the daytime hours when ship traffic is more frequent and average ship length and displacement increase. The lowest power occurs during the late-night and early-morning hours, when containership traffic decreases because of darkness. Shipping is a unique example of long-period “cultural” noise related to human activity; cultural seismic noise is generally at shorter periods (0.1–1 s) [McNamara and Buland, 2004].

5.3. Wind

[26] Wind is a ubiquitous mechanism for disturbing open water surfaces and generating standing waves in enclosed bodies of water [Stevens and Lawrence, 1997]. Figure 11 shows wind speed observations recorded digitally at 15 min intervals from a Young anemometer at a height of 48 m, on a nearby weather tower on BCI (Figure 1c) [Windsor, 1990] during the same interval as our seiche observations taken when both the seismic station (CU.BCIP) and water level meter also were operating (1 March 2008). As expected from common global wind patterns, a clear diurnal variation is

observed, with the highest wind speeds during the daytime hours, peaking at noon, and the lowest during the night (Figure 11). Thus, higher winds as well as ship traffic correlate with high seiche and long-period seismic amplitudes. High-speed winds can cause water to pile up toward one side of a basin and then seek to establish a state of hydrostatic equilibrium in response to gravity, driving a seiche. Similarly, pressure variations associated with winds can depress or elevate water surfaces directly.

[27] Previous studies have attributed the formation of seiches in lakes in British Columbia, Canada, and Lake Gatun to wind. *Stevens and Lawrence* [1997] found that wind correlates best with fundamental mode seiche amplitude in several lakes in British Columbia. *Keller and Stallard* [1994] found that methane gas emissions in Lake Gatun are strongly correlated with wind speed and suggested that wind induced wave motions cause internal currents and pressure fluctuations sufficient to disturb sediments and release methane bubbles. In a more recent study, using a similar data set from Lake Gatun and lakes in Puerto Rico, *Joyce and Jewell* [2003] demonstrate that periods of methane bubbling have a higher correlation with current velocity than with wind velocity, implying a causal link with seiching. They also suggest that internal currents and seiching resulting from nonwind disturbances, such as ships, produce bottom shearing sufficient to drive methane release from sediments.

[28] At this point, we have demonstrated only correlations between seismic amplitude, seiche height, and these two likely forcing mechanisms (wind and shipping) while the causality remains less clear. Nevertheless, we think it likely that internal currents and seiching are induced in some proportions by both forcing mechanisms and possibly others; which mechanism(s) dominate is a subject for further study.

6. Conclusions

[29] The problem of oscillating water in enclosed bays and harbors, generating strong unpredictable currents, is of great practical significance to the degree they affect the safety of travelling and moored vessels. Seiches are neither well understood nor well monitored. A better understanding of seiche behavior and forcing mechanisms could contribute to improved estimates of potential hazard to vulnerable shipping, communities, and infrastructure. The observation of seiching in the Panama Canal suggests that seismic instrumentation could contribute to seiche monitoring and potentially contribute to improved estimates of flooding hazard to vulnerable infrastructure and improved understanding of the distribution of contaminants and methane in lake ecosystems.

[30] Ambient noise studies are important for assessing seismic station performance, particularly at the longest (and shortest) periods, where the noise can be comparable to earthquake shaking. We have demonstrated that small changes in local ground tilt at GSN station CU.BCIP can be the largest seismic signal from 100–200 s period. This long-period seismic energy is likely due to tilt induced by a seiche in the Panama Canal main channel north of BCI. Wind and ships are potential drivers for this recorded seiche activity, in that both correlate well with the diurnal variation in seiche height. However, given our limited observations, we are unable to determine whether shipping traffic, wind and/or wind pressure is the primary forcing mechanism in the for-

mation of the Panama Canal seiche. It is likely that both shipping and wind contribute to some extent and it would be of practical value to understand these forcing phenomena in greater detail.

[31] While the mechanism of seiche formation is not yet clear, seiching clearly is behind the observed long-period seismic signal at CU.BCIP. As a result, we propose a new passive-seismic method for seiche monitoring utilizing existing infrastructure such as the GSN. Seismic monitoring may improve our ability to predict seiche events of concern. Along with tsunamis and atmospheric waves, the NEIC records seiching observations induced by earthquakes as part of its earthquake catalog because larger seiches pose a human hazard.

[32] The methods discussed in this paper provide a first step toward using seismic observations to improve understanding of seiche dynamics. In addition, the methods and observations discussed in this paper provide a first step toward quantifying the impact of water inundation as recorded by seismometers. This type of quantified understanding of water will help in future estimates of similar phenomena such as the seismic observations of tsunami impact [*Okal*, 2007; *Yuan et al.*, 2005].

[33] **Acknowledgments.** The authors have numerous contributors to thank, including the CU.BCIP scouting and construction crews that included J. McMillan, J. Weaver, D. Anderson, and M. Robertson, ASL QC expert L. D. Sandoval (for reviewing the seismic data), and J. Gallegos for his help in configuring and retrieving data from the HOB0 water depth logger. B. Heap and L. Blair provided and mapped Panama Canal water depth data for Figure 1. The authors also are grateful to partners in the operation of CU.BCIP including B. Birmingham (STRI) and E. Camacho (UPAN). The authors benefited from conversations with many researchers, including J. Amundson, S. O'Neel, V. Tsai, A. Hutko, K. Koper, P. Bromirski, J. McNamara, B. Stallard, E. Okal, R. Aster, and J. Love. Analysis and mapping software used includes PQLX [*Boaz and McNamara*, 2008; *McNamara and Boaz*, 2011], SAC [*Goldstein and Snoke*, 2005], GMT [*Wessel and Smith*, 1991] and Matlab. Finally, detailed and thoughtful comments were provided by USGS reviewer G. Hayes as well as 2 anonymous JGR reviewers. We especially want to acknowledge contributions from J. Evans that greatly improved this manuscript.

References

- Ahern, T., R. Casey, D. Barnes, R. Benson, and T. Knight (2007), SEED reference manual, version 2.4, Inc. Res. Inst. for Seismol., Seattle, Wash.
- Aster, R., D. McNamara, and P. Bromirski (2008), Multi-decadal climate-induced oceanic microseism variability, *Seismol. Res. Lett.*, *79*(2), 194–202.
- Aster, R. C., D. E. McNamara, and P. D. Bromirski (2010), Global trends in extremal microseism intensity, *Geophys. Res. Lett.*, *37*, L14303, doi:10.1029/2010GL043472.
- Boaz, R. I., and D. E. McNamara (2008), PQLX, a data quality control system: Uses and applications, *Obs. and Res. Facil. for Eur. Seismol.*, De Bilt, Netherlands.
- Bromirski, E. V. (2009), Earth vibrations, *Science*, *324*, 1026–1027.
- Bromirski, P., and F. Duennebier (2002), The near-coastal microseism spectrum: Spatial and temporal wave climate relationships, *J. Geophys. Res.*, *107*(B8), 2166, doi:10.1029/2001JB000265.
- Ekström, G. (2001), Time domain analysis of Earth's long-period background seismic radiation, *J. Geophys. Res.*, *106*, 26,483–26,493, doi:10.1029/2000JB000086.
- Foster, H., and T. Karlstrom (1967), The Alaska earthquake, March 27, 1964: Region effects. Ground breakage and associated effects in the Cook Inlet, Alaska, resulting from the March 27, 1964, earthquake, *Prof. Pap. 543-F*, U.S. Geol. Surv., Washington, D. C.
- Goldstein, P., and A. Snoke (2005), SAC availability for the IRIS community, *Rep. UCRL-JRNL-211140*, Inc. Res. Inst. for Seismol., Seattle, Wash. [Available at <http://www.iris.edu/news/newsletter/vol7no1/page1.htm>.]
- Hasselmann, K. (1963), A statistical analysis of the generation of microseisms, *Rev. Geophys.*, *1*(2), 177–210, doi:10.1029/RG001i002p00177.

- Ichinose, G. A., J. G. Anderson, K. Satake, R. A. Schweichert, and M. M. Lahren (2000), The potential hazard from tsunami and seiche waves generated by large earthquakes within Lake Tahoe, California-Nevada, *Geophys. Res. Lett.*, *27*, 1203–1206, doi:10.1029/1999GL011119.
- Joyce, J., and P. Jewell (2003), Physical controls on methane ebullition from reservoirs and lakes, *Environ. Eng. Geosci.*, *9*(2), 167–178, doi:10.2113/9.2.167.
- Kedar, S., M. Longuet-Higgins, F. Webb, N. Graham, R. Clayton, and C. Jones (2008), The origin of deep ocean microseisms in the North Atlantic Ocean, *Proc. R. Soc. A*, *464*, 777–793, doi:10.1098/rspa.2007.0277.
- Keller, M., and R. Stallard (1994), Methane emission by bubbling from Gatun Lake, Panama, *J. Geophys. Res.*, *99*, 8307–8319, doi:10.1029/92JD02170.
- Longuet-Higgins, M. S. (1950), A theory of the origin of microseisms, *Philos. Trans. R. Soc. London A*, *243*, 1–35.
- McMillan, J. (2002), Methods of installing United States National Seismographic Network (USNSN) stations: A construction manual, *Open File Rep. 02-0144*, U.S. Geol. Surv., Washington, D. C.
- McNamara, D. E., and R. I. Boaz (2011), PQLX: A seismic data quality control system description, applications, and users manual, *Open File Rep. 2010-1292*, 41 pp., U.S. Geol. Surv., Washington, D. C.
- McNamara, D., and R. Buland (2004), Ambient noise levels in the continental United States, *Bull. Seismol. Soc. Am.*, *94*, 1517–1527, doi:10.1785/012003001.
- McNamara, D., J. McCarthy, and H. Benz (2006), Improving earthquake and tsunami warning for the Caribbean Sea, Gulf of Mexico and the Atlantic coast, *Fact Sheet 2006-3012*, U.S. Geol. Surv., Washington, D. C. [Available at <http://pubs.usgs.gov/fs/2006/3012/>.]
- McNamara, D. E., C. R. Hutt, L. S. Gee, R. P. Buland, and H. M. Benz (2009), A method to establish seismic noise baselines for automated station assessment, *Seismol. Res. Lett.*, *80*(4), 628–637, doi:10.1785/gssrl.80.4.628.
- Merian, J. R. (1828), *Über die Bewegung Tropbarer Flüssigkeiten in Gefassen*, Basel, Switzerland.
- Okal, E. A. (2007), Seismic records of the 2004 Sumatra and other tsunamis: A quantitative study, *Pure Appl. Geophys.*, *164*, 325–353, doi:10.1007/s00024-006-0181-4.
- Pabst, A. F. (2000), Some history and hydrology of the Panama Canal, *Tech. Pap. TP-159*, U.S. Army Corps of Eng., Washington, D. C.
- Peterson, J. (1993), Observation and modeling of seismic background noise, *Open File Rep. 93-322*, U.S. Geol. Surv., Washington, D. C.
- Rhie, J., and B. Romanowicz (2004), Excitation of Earth's continuous free oscillations by atmosphere-ocean-seafloor coupling, *Nature*, *432*, 552–556.
- Rueda, F., and S. G. Schladow (2002), Surface seiches in lakes of complex geometry, *Limnol. Oceanogr.*, *47*, 906–910, doi:10.4319/lo.2002.47.3.0906.
- Simojoki, H. (1961), On seiches in some lakes in Finland, *Geophysica*, *7*(3), 145–150.
- Stevens, C. L., and G. A. Lawrence (1997), Estimation of wind-forced internal seiche amplitudes in lakes and reservoirs, with data from British Columbia, Canada, *Aquat. Sci.*, *59*, 115–134, doi:10.1007/BF02523176.
- Turcotte, D. L., and G. Schubert (2002), *Geodynamics*, 2nd ed., 456 pp., Cambridge Univ. Press, Cambridge, U. K.
- Velegrakis, A. F., M. I. Voutsoukas, A. M. Vagenas, T. Karambas, K. Dimou, and T. Zarkadas (2007), Field observations of waves generated by passing ships: A note, *Coastal Eng.*, *54*, 369–375, doi:10.1016/j.coastaleng.2006.11.001.
- Wessel, P., and W. Smith (1991), Free software helps display data, *Eos Trans. AGU*, *72*(41), 441, doi:10.1029/90EO00319.
- Windsor, D. M. (1990), *Climate and Moisture Variability in a Tropical Forest: Long-Term Records From Barro Colorado Island, Panama*, Smithsonian. Inst. Press, Washington, D. C.
- Yanagisawa, M. (1980), Observations of seiche-related tilt in the Aburatsubo Observatory, *Bull. Earthquake Res. Inst. Univ. Tokyo*, *55*, 331–345.
- Yuan, X., R. Kind, and H. A. Pedersen (2005), Seismic monitoring of the Indian Ocean tsunami, *Geophys. Res. Lett.*, *32*, L15308, doi:10.1029/2005GL023464.

L. S. Gee, C. R. Hutt, D. E. McNamara, and A. T. Ringler, Albuquerque Seismological Laboratory, USGS, 1711 Illinois St., Golden, CO 94550, USA. (mcnamara@usgs.gov)